of cats (*41*) and in the amygdaloid complex of rats, which expresses both slow and fast rhythms (but no ripple-like events during SWS) (*42*). Conversely, rat hippocampal firing patterns during cortical slow waves (*43*) resemble the cortical firing in *Pogona* around DVR sharp waves. Further work is thus needed to clarify the relationship between DVR, a dominant part of the reptilian forebrain, and its potential mammalian equivalent (*44*).

Recent work on mammalian hippocampal ripples focuses on their potential importance for memory transfer and consolidation through accelerated replay of awake-state activity and activation of synaptic plasticity rules in cortical targets (*32*, *33*). In rats, correlations between CA1 ripples and cortical spindles have been demonstrated (*26*). Our results in a reptile suggest that there is also a functional relationship between the DVR and cortex. The projections between the DVR and cortex are extensive, direct, and reciprocal. This offers an opportunity to test the potential generality of the principle whereby sleep ripples participate in memory transfer and consolidation. More generally, the existence of sleep-related dynamics in the brains of reptiles may shed new light on general principles of information processing during sleep.

REFERENCES AND NOTES

1. A. P. Vorster, J. Born, *Neurosci. Biobehav. Rev.* **50**, 103–119 (2015).
2. R. Allada, J. M. Siegel, *Curr. Biol.* **18**, R670–R679 (2008).
3. R. V. Rial *et al*., *Neurosci. Biobehav. Rev.* **34**, 1144–1160 (2010).
4. C. Smith, *Neurosci. Biobehav. Rev.* **9**, 157–168 (1985).
5. J. E. Zimmerman, N. Naidoo, D. M. Raizen, A. I. Pack, *Trends Neurosci.* **31**, 371–376 (2008).
6. D. Bushey, G. Tononi, C. Cirelli, *Science* **332**, 1576–1581 (2011).
7. P. S. Low, S. S. Shank, T. J. Sejnowski, D. Margoliash, *Proc. Natl. Acad. Sci. U.S.A.* **105**, 9081–9086 (2008).
8. R. J. Greenspan, G. Tononi, C. Cirelli, P. J. Shaw, *Trends Neurosci.* **24**, 142–145 (2001).
9. A. L. Loomis, E. N. Harvey, G. A. Hobart III, *J. Exp. Psychol.* **21**, 127–144 (1937).
10. E. Aserinsky, N. Kleitman, *Science* **118**, 273–274 (1953).
11. M. Jouvet, *Prog. Brain Res.* **18**, 20–62 (1965).
12. R. E. Brown, R. Basheer, J. T. McKenna, R. E. Strecker, R. W. McCarley, *Physiol. Rev.* **92**, 1087–1187 (2012).
13. M. Monnier, *Experientia* **36**, 16–19 (1980).
14. N. C. Rattenborg, *Brain Res. Bull.* **69**, 20–29 (2006).
15. N. C. Rattenborg, D. Martinez-Gonzalez, J. A. Lesku, *Neurosci. Biobehav. Rev.* **33**, 253–270 (2009).
16. J. M. Siegel, *Trends Neurosci.* **31**, 208–213 (2008).
17. R. V. Rial *et al*., *Brain Res. Bull.* **72**, 183–186 (2007).
18. P. A. Libourel, A. Herrel, *Biol. Rev. Camb. Philos. Soc.* (2015).
19. J. A. Hobson, *Nature* **437**, 1254–1256 (2005).
20. W. F. Flanigan Jr., *Brain Behav. Evol.* **8**, 401–416 (1973).
21. K. Hartse, in *Principles and Practice of Sleep Medicine*, M.H. Kryger, T. Roth, D.W. Dement, Eds. (Elsevier Saunders, ed. 2, 1994), pp. 95–104.
22. F. Ayala-Guerrero, G. Mexicano, *Comp. Biochem. Physiol. A* **151**, 305–312 (2008).
23. G. F. Striedter, *J. Comp. Neurol.* **524**, 496–517 (2016).
24. The animals, which were raised in controlled feeding, light, and temperature conditions (see the materials and methods section in the supplementary materials), were observed continuously by means of video and physiological monitoring over epochs of 18 to 20 hours in a familiar experimental arena. Light-dark cycles were identical and synchronized to those in their home terrarium. About 1 to 2 hours before normal nighttime (daylight off), the lizards spontaneously became drowsy, settled in one location, and started closing their eyes intermittently (Fig. 1B). During this pre-sleep phase, axial and limb postural tone decreased until the animals assumed a fully relaxed, horizontal sleeping posture with their heads resting on the floor. Their cardiac rhythms decreased over 1 to 2 hours from 40 to 60 beats per minute (bpm) in the awake state to 20 to 30 bpm, by which time their eyes were closed. A low heart rate was maintained throughout the night, except for occasional peaks correlated with brief body repositioning. Toward the end of the night, the lizards' postural tone increased, and they slowly lifted their heads; they opened their eyes, intermittently at first, then reliably at or shortly after the onset of light (Fig. 1B).
25. J. Voigts, J. H. Siegle, D. L. Pritchett, C. I. Moore, *Front. Syst. Neurosci.* **7**, 8 (2013).
26. A. G. Siapas, M. A. Wilson, *Neuron* **21**, 1123–1128 (1998).
27. J. O'Keefe, *Exp. Neurol.* **51**, 78–109 (1976).
28. G. Buzsáki, Z. Horváth, R. Urioste, J. Hetke, K. Wise, *Science* **256**, 1025–1027 (1992).
29. G. Buzsáki, *Hippocampus* **25**, 1073–1188 (2015).
30. A. Draguhn, R. D. Traub, D. Schmitz, J. G. Jefferys, *Nature* **394**, 189–192 (1998).
31. J. M. Siegel, in *Principles and Practice of Sleep Medicine*, M. H. Kryger, T. Roth, W. C. Dement, Eds. (Elsevier Saunders, ed. 4, 2005), pp. 120–135.
32. D. J. Foster, M. A. Wilson, *Nature* **440**, 680–683 (2006).
33. M. A. Wilson, B. L. McNaughton, *Science* **265**, 676–679 (1994).
34. J. Lu, D. Sherman, M. Devor, C. B. Saper, *Nature* **441**, 589–594 (2006).
35. F. Weber *et al*., *Nature* **526**, 435–438 (2015).
36. J. A. Hobson, R. W. McCarley, P. W. Wyzinski, *Science* **189**, 55–58 (1975).
37. Y. Hayashi *et al*., *Science* **350**, 957–961 (2015).
38. C. B. Saper, T. C. Chou, T. E. Scammell, *Trends Neurosci.* **24**, 726–731 (2001).
39. C. B. Saper, T. E. Scammell, J. Lu, *Nature* **437**, 1257–1263 (2005).
40. R. G. Northcutt, *Annu. Rev. Neurosci.* **4**, 301–350 (1981).
41. F. Grenier, I. Timofeev, M. Steriade, *J. Neurophysiol.* **86**, 1884–1898 (2001).
42. D. Paré, D. R. Collins, J. G. Pelletier, *Trends Cogn. Sci.* **6**, 306–314 (2002).
43. A. Sirota, J. Csicsvari, D. Buhl, G. Buzsáki, *Proc. Natl. Acad. Sci. U.S.A.* **100**, 2065–2069 (2003).
44. H. J. Karten, *Brain Behav. Evol.* **38**, 264–272 (1991).

ACKNOWLEDGMENTS

This research was funded by the Max Planck Society and the European Research Council (G.L.) and by fellowships from the Minerva Foundation (M.S.-I.) and the Swiss National Science Foundation (J.M.O.). The code for analysis and partial data are available at www.brain.mpg.de/sheinidelsonetal2016, and the full primary data are available from G.L. on request. The authors are grateful to G. Wexel for help in surgery and postoperative care; M. Klinkmann, A. Arends, Á. M. Pardo, T. Manthey, and C. Thum for technical assistance; F. Baier, T. Maurer, G. Schmalbach, and A. Umminger for help with mechanical design and fabrication; N. Heller for help with electronics; K. Schröder and C. Schürmann (Goethe University Medical School, Institute for Cardiovascular Physiology) for help with μ-CT scanning of lizards; the animal caretaker crew for lizard care; and T. Tchumatchenko, H. Ito, M. Kaschube, E. Schuman, A. Siapas, and the Laurent laboratory for their suggestions during the course of this work or on the manuscript.

SUPPLEMENTARY MATERIALS

www.sciencemag.org/content/352/6285/590/suppl/DC1
Materials and Methods
Figs. S1 to S10
References (*45*–*53*)
Movie S1

29 January 2016; accepted 1 April 2016
10.1126/science.aaf3621

SIGNAL TRANSDUCTION

Phase separation of signaling molecules promotes T cell receptor signal transduction

Xiaolei Su,[1,2]* Jonathon A. Ditlev,[1,3]* Enfu Hui,[1,2] Wenmin Xing,[1,3] Sudeep Banjade,[1,3] Julia Okrut,[1,2] David S. King,[4] Jack Taunton,[1,2] Michael K. Rosen,[1,3]† Ronald D. Vale[1,2]†

Activation of various cell surface receptors triggers the reorganization of downstream signaling molecules into micrometer- or submicrometer-sized clusters. However, the functional consequences of such clustering have been unclear. We biochemically reconstituted a 12-component signaling pathway on model membranes, beginning with T cell receptor (TCR) activation and ending with actin assembly. When TCR phosphorylation was triggered, downstream signaling proteins spontaneously separated into liquid-like clusters that promoted signaling outputs both in vitro and in human Jurkat T cells. Reconstituted clusters were enriched in kinases but excluded phosphatases and enhanced actin filament assembly by recruiting and organizing actin regulators. These results demonstrate that protein phase separation can create a distinct physical and biochemical compartment that facilitates signaling.

Many cell surface receptors and downstream signaling molecules coalesce into micrometer- or submicrometer-sized clusters upon initiation of signaling (*1*, *2*). However, the effect of this clustering on signal transduction is poorly understood. T cell receptor (TCR) signaling is a well-studied example of this general phenomenon (*3*). TCR signaling proceeds through a series of biochemical reactions that can be viewed as connected modules. In the upstream module, the TCR is phosphorylated by Lck, a membrane-bound protein kinase of the Src family. TCR phosphorylation is opposed by a transmembrane phosphatase, CD45 (*3*). The phosphorylated cytoplasmic domains of the TCR complex recruit and activate the cytosolic tyrosine kinase ZAP70 (*4*). In the intermediate module, ZAP70 phosphorylates the transmembrane protein LAT (linker for activation of T cells) on multiple tyrosine residues. These phosphotyrosines

are binding sites for adapter proteins Grb2 and Gads, which further interact with Sos1 [a guanine nucleotide exchange factor (GEF) for the small guanosine triphosphatase Ras] or SLP-76 (another adaptor in TCR signaling). Components of the LAT complex activate several downstream modules that mediate calcium mobilization, mitogen-activated protein kinase (MAPK) activation, and actin polymerization (*5*, *6*).

LAT and its binding partners coalesce into micrometer- or submicrometer-sized clusters at the plasma membrane upon TCR activation (*7*–*10*). Elimination of these microclusters by deletion of key components (for example, LAT or Grb2) impairs downstream signaling and transcriptional responses (*5*, *11*). However, effects due to loss of clusters have not been distinguished from those due to loss of component molecules. Nor do we understand the changes in biochemistry and consequent signaling that emerge specifically when signaling molecules are organized from an unclustered to a clustered state (*12*).

To explore the mechanism of formation and functional consequences of T cell microclusters, we reconstituted a TCR signaling pathway from purified components. To substitute for the plasma membrane, we used supported bilayers composed of a defined, simple lipid composition. We initially reconstituted the intermediate module of the TCR signaling cascade, composed of phosphorylated LAT (pLAT), Grb2, and Sos1. Multivalent interactions between these proteins (Fig. 1A) are thought to drive the formation of signaling microclusters on the T cell membrane (*8*, *13*), although direct experimental evidence for the sufficiency of this mechanism has been lacking. We prepared fluorescently labeled pLAT, containing the four C-terminal phosphotyrosine residues that are sufficient for TCR signaling (*14*); this pLAT also contains an N-terminal His_8 tag that allowed its attachment to Ni^{2+}-containing supported lipid bilayers (*15*). pLAT was uniformly distributed (Fig. 1B) and freely diffused on the lipid bilayer (movie S1). Upon addition of Grb2 and Sos1, submicrometer-sized clusters formed within 1 min and gradually grew in size. Cluster formation required tyrosine phosphorylation of LAT (fig. S1D).

[1]Howard Hughes Medical Institute (HHMI) Summer Institute, Marine Biological Laboratory, Woods Hole, MA 02543, USA. [2]Department of Cellular and Molecular Pharmacology and Howard Hughes Medical Institute, University of California, San Francisco, CA 94158, USA. [3]Department of Biophysics and Howard Hughes Medical Institute, University of Texas Southwestern Medical Center, Dallas, TX 75390, USA. [4]HHMI Mass Spectrometry Laboratory and Department of Molecular and Cellular Biology, University of California, Berkeley, CA 94720, USA.
*These authors contributed equally to this work. **†Corresponding author. Email: ron.vale@ucsf.edu (R.D.V.); michael.rosen@utsouthwestern.edu (M.K.R.)**

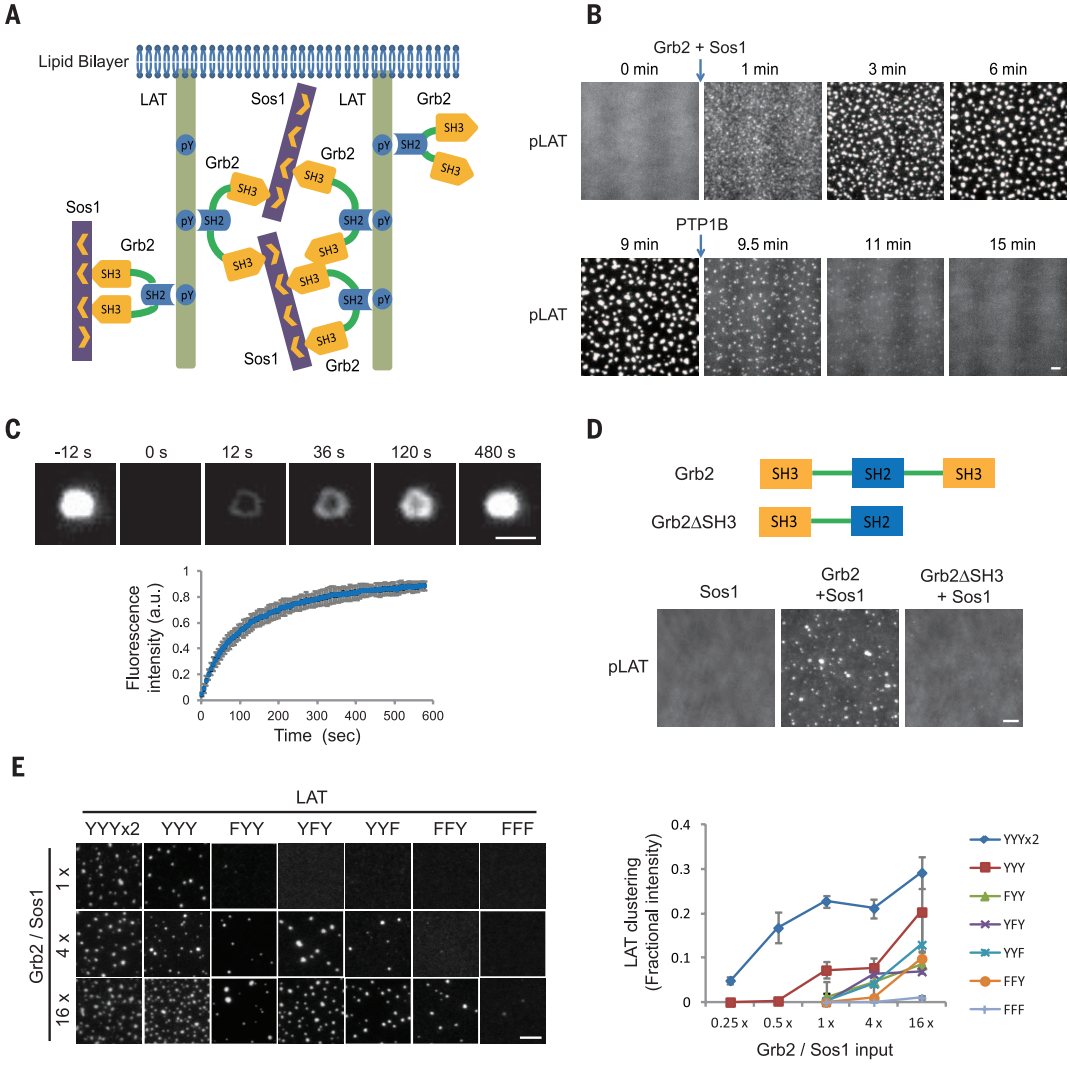

Fig. 1. Multivalent interactions drive LAT cluster formation. (**A**) Schematic of the proteins and interactions in the clustering assay. (**B**) Total internal reflection fluorescence microscopy (TIRF) imaging of LAT clustering and declustering. Clusters formed after adding Grb2 (0.5 μM) and Sos1 (the proline-rich motifs) (0.25 μM) to membrane-bound pLAT-Alexa488 (1000 molecules/μm^2) at 0 min and dissolved after adding the protein tyrosine phosphatase PTP1B (2 μM) at 9 min. Scale bar, 2 μm. See movie S2. (**C**) FRAP of clustered pLAT on planar lipid bilayers; time 0 indicates the time of the photobleaching pulse. The bottom plot shows the time course of the recovery of pLAT clusters formed with 1 μM Grb2 and 2 μM Sos1. Shown are the mean ± SD. $N = 7$ pLAT clusters. Scale bar, 2 μm. (**D**) TIRF imaging of pLAT-Alexa488 (300 molecules/μm^2) with Sos1 (0.5 μM) alone or additionally with wild-type Grb2 (0.5 μM) or Grb2ΔSH3 (1 μM) (concentrations were set to maintain identical total SH3 concentrations in the experiments containing Grb2 and Grb2ΔSH3). Scale bar, 2 μm. (**E**) Valency-dependent clustering of pLAT. (Left) pLAT wild-type with three Grb2 phosphorylation sites (YYY) or mutants that contain six (2xYYY), two (FYY, YFY, and YYF), one (FFY), or zero (FFF) phosphotyrosines were incubated with increasing concentrations of Grb2 and Sos1. 1x indicates 125 nM Grb2 and 62 nM Sos1. pLAT valency mutants were plated at a density of ~300 molecules/μm^2. Clusters were imaged by TIRF microscopy. Scale bar, 5 μm. (Right) Quantification of clustering of pLAT valency mutants. Clustering degree was quantified by fractional intensity. Phase diagrams of pLAT mutants using a larger range of Grb2 and Sos1 concentrations are shown in fig. S5. Values shown are the mean ± SD. $N = 3$ independent experiments.

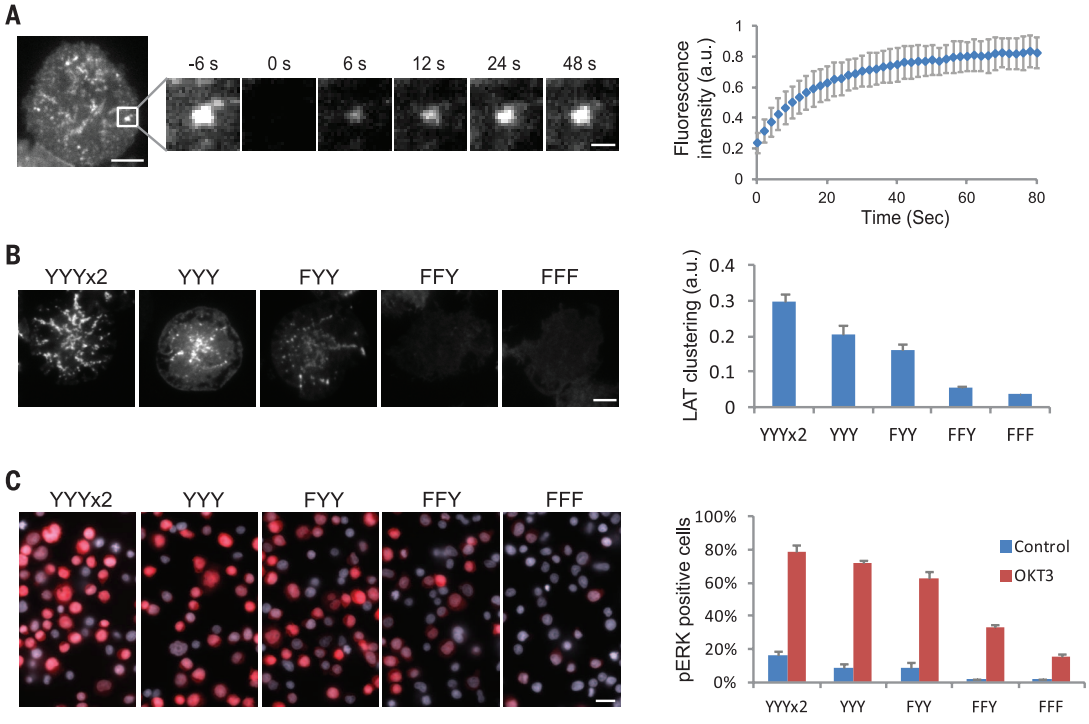

Fig. 2. LAT clustering promotes MAPK(ERK) signaling in T cells. (**A**) FRAP of LAT-mCitrine clusters on plasma membranes of Jurkat T cells activated by plate-presented antibody to CD3 (OKT3 at 5 μg/mL); time 0 indicates the time of the photobleaching pulse. Scale bar, 5 μm or 1 μm on the enlarged panel. Right plot shows the time course of the recovery (mean ± SD) of 15 cells. (**B**) TIRF microscopy revealed cluster formation of LAT variants in activated T cells. A LAT-deficient line (Jcam2.5) stably expressing LAT variants containing six (2x YYY), three (YYY), two (FYY), one (FFY), or zero (FFF) tyrosines for Grb2 binding was activated by plate-presented OKT3 at 5 μg/mL. See the supplementary materials for clustering quantification. Scale bar, 5 μm. Shown are mean ± SEM. $N = 16$ to 20 cells. (**C**) MAPK(ERK) activation in Jurkat T cells expressing LAT valency mutants. Cells were activated by OKT3 at 5 μg/mL, fixed at 10 min, and stained with an antibody to phosphorylated ERK (red) and a nucleus dye Hoechst (blue). Scale bar, 20 μm. Right plot shows the percentage of pERK positive cells. About 200 to 300 cells were scored for each data point. Shown are mean ± SEM. $N = 3$ independent experiments.

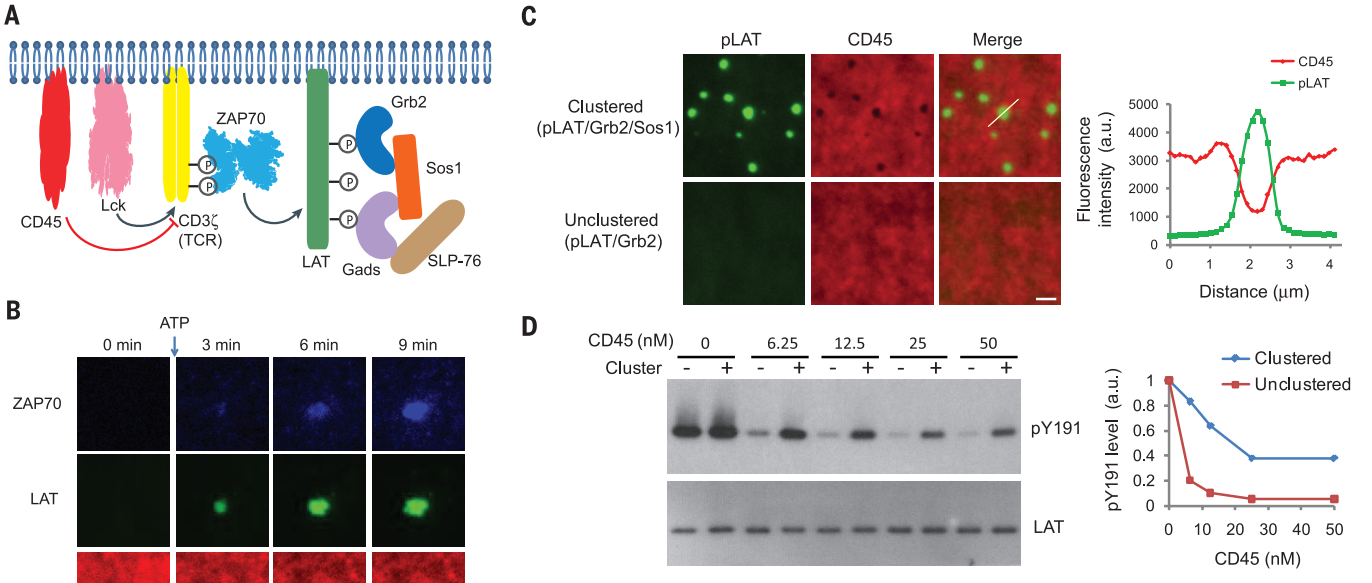

Fig. 3. Reconstitution of TCR phosphorylation to LAT clustering. (**A**) Schematic of components in a reaction designed to reconstitute signaling from TCR/CD3ζ phosphorylation to LAT clustering. The cytoplasmic domains of CD45, Lck, CD3ζ, and LAT were polyhistidine-tagged for membrane attachment and incubated with other components in solution. ATP was added to trigger the phosphorylation cascade. Input: CD45-SNAP-TMR, Lck, CD3ζ, and LAT-Alexa647 at 30, 250, 500, and 1000 molecules/μm^2, respectively; 10 nM ZAP70-505-Star; 250 nM Grb2; 125 nM Sos1; 250 nM Gads; 125 nM SLP-76; and 0.5 mM ATP-Mg. (**B**) TIRF microscopy revealed time courses of ZAP70 membrane recruitment, CD45 exclusion, and LAT clustering in the reconstituted pathway. A larger field view of LAT clusters is shown in fig. S6B. Scale bar, 2 μm. (**C**) (Left) pLAT-Alexa488 (300 molecules/μm^2) bound to planar lipid bilayers was incubated with Grb2 (1 μM) in the presence (top) or absence (bottom) of Sos1 (1 μM). Then the cytoplasmic domain of CD45-TMR (4 nM, with an N-terminal His_{10} tag) was added, and its localization was visualized by TIRF microscopy. Scale bar, 2 μm. (Right) Quantification of fluorescence intensity of pLAT and CD45 along the line scan indicated by a white line in the top merged image. (**D**) Western blot analysis of pLAT dephosphorylation by CD45. pLAT bound to membrane (300 molecules/μm^2) was incubated with 1 μM Grb2 (unclustered pLAT) or 1 μM Grb2 plus 1 μM Sos1 (clustered pLAT). His_{10}-CD45 was then added, and the reactions were stopped after 5 min by adding SDS–polyacrylamide gel electrophoresis loading buffer containing 2 mM vanadate. Quantification of pLAT phosphorylation normalized to the total LAT signal is shown in the right plot.

Furthermore, dephosphorylation of pLAT by high concentrations of the soluble protein tyrosine phosphatase 1B (PTP1B, 2 μM) caused the clusters to disassemble (Fig. 1B and movie S2). pLAT, Grb2, and Sos1 all colocalized within clusters, and clusters did not form if either Grb2 or Sos1 was omitted (fig. S1, E and F). pLAT also clustered with Gads and SLP-76, two other components of LAT clusters (*6*, *7*), but less efficiently than with Grb2 and Sos1 (fig. S2, A and B). Clustering efficiency, however, increased dramatically with the addition of Nck (fig. S2C), an adaptor protein known to link SLP-76 to actin regulators (*16*).

pLAT, Grb2, and Sos1 clusters exhibited dynamic liquid-like properties. The rounded edges of clusters fluctuated (extending and retracting) on a time scale of seconds, and clusters sometimes fused with one another (movie S2). pLAT molecules exchanged into and out of clusters, as revealed by fluorescence recovery after photobleaching (FRAP) (Fig. 1C). Single pLAT molecules diffused rapidly outside of clusters but slowly within them (fig. S3, A to C). We also observed capture and release of single molecules by clusters (movie S3). These results show that pLAT microclusters are liquid-like, phase-separated structures (*17*, *18*) on membranes.

Both SH3 domains of Grb2 were required for cluster formation, indicating a role of protein cross-bridging by this adaptor protein (Fig. 1D and fig. S4A). Clustering initially increased with increasing pLAT density but then decreased at higher pLAT densities on the membrane (fig. S4B), consistent with a theoretical multivalent interaction model (*19*). The valency of phosphotyrosines on LAT also affected clustering efficiency. Three of the four distal phosphotyrosines in LAT are recognized by the SH2 domain of Grb2 (*20*). Clustering in vitro progressively decreased by mutating one, two, or all three tyrosines and was enhanced by doubling the number of

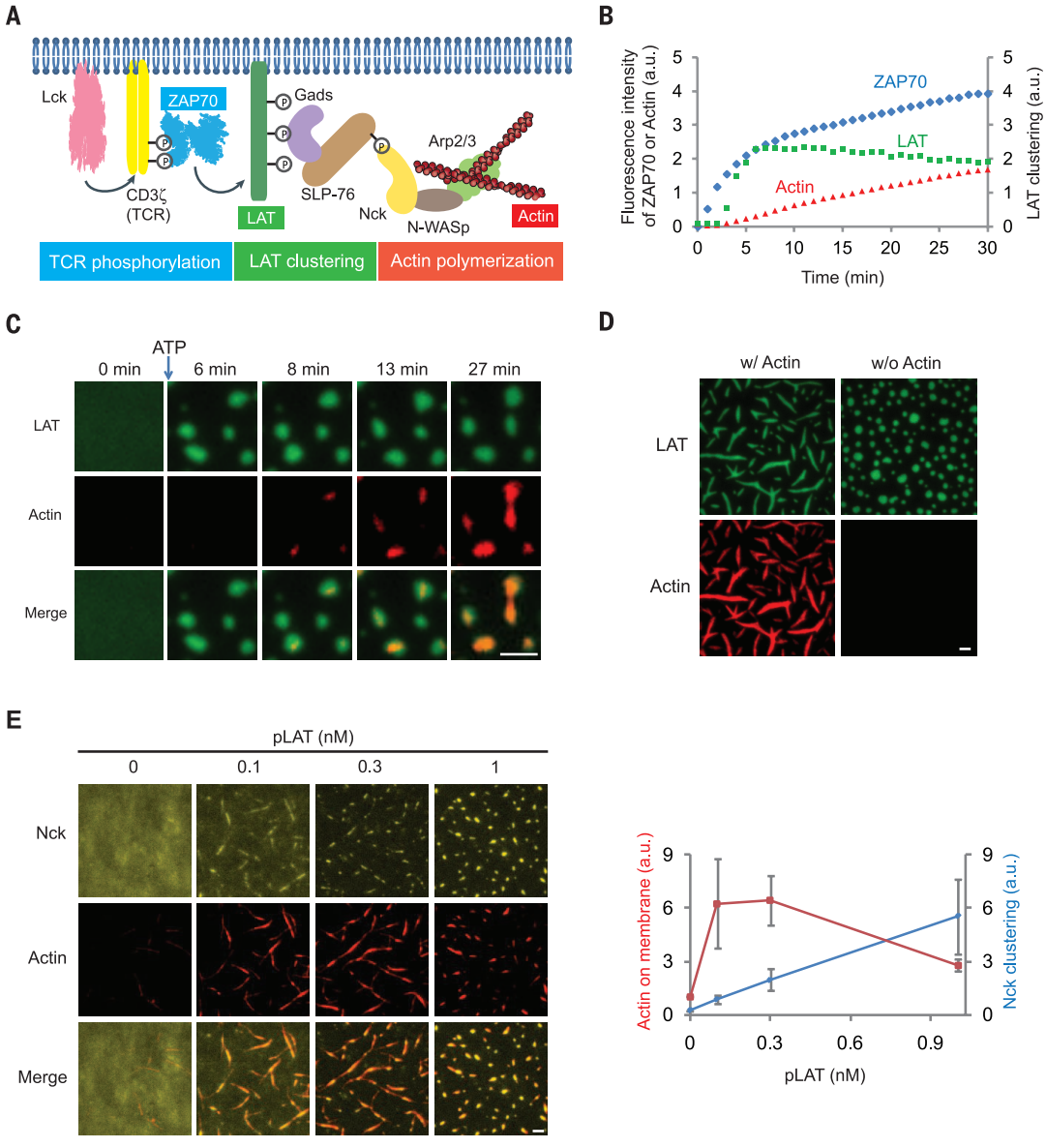

Fig. 4. LAT clustering promotes actin polymerization. (**A**) Schematic of the reconstituted signaling pathway from CD3ζ/TCR phosphorylation to actin polymerization. ZAP70-505-Star, LAT-Alexa647, and actin-rhodamine serve as reporters for TCR phosphorylation, LAT clustering, and actin assembly, respectively. Lck, CD3ζ, and LAT were membrane-attached through a polyhistidine tag and incubated with other components in solution. ATP was then added to trigger the signaling cascade. Input: same for Lck, CD3ζ, pLAT-Alexa647, and ZAP70-505-Star as described in Fig. 3A. The rest are 250 nM Gads, 125 nM SLP-76, 500 nM Nck, 250 nM N-WASP, 2.5 nM Arp2/3 complex, 500 nM actin (5% rhodamine labeled), and 0.5 mM ATP-Mg. (**B**) Time courses of ZAP70 membrane recruitment, LAT clustering, and actin polymerization in the reconstituted assay after addition of ATP at time 0. LAT clustering was quantified as variance of fluorescence intensities on membranes (see the supplementary materials). (**C**) TIRF imaging showing actin assembly on the LAT clusters. Scale bar, 2 μm. (**D**) TIRF imaging of pLAT-Alexa647 and actin-rhodamine 45 min after adding ATP to the reaction. Input: same as in Fig. 4A except with higher concentrations of components of actin and actin regulators [500 nM SLP-76, 1000 nM Nck, 500 nM N-WASP, 5 nM Arp2/3 complex, 1000 nM actin (5% rhodamine-labeled)]. Scale bar, 2 μm. (**E**) (Left) TIRF microscopy images of His_{10}-Nck-Pacific Blue and actin-rhodamine on the bilayer. Nck (150 molecules/μm^2) was attached to the bilayer, and N-WASP (5 nM), Arp2/3 complex (0.25 nM), actin (200 nM, 5% rhodamine labeled), and 0.5 mM ATP-Mg were in solution. Increasing concentrations of His-tagged pLAT were added as indicated, along with Gads and pSLP-76. At 0.1 nM pLAT, Gads and pSLP-76 concentrations were 8 nM and 4 nM, respectively. As pLAT concentration was increased, more Gads and pSLP-76 were added to maintain a constant ratio of the clustering components. Scale bar, 2 μm. (Right) Mean actin fluorescence (red) and Nck clustering level (blue), quantified as variance of His_{10}-Nck fluorescence intensity, are plotted for increasing concentrations of pLAT. Shown are mean ± SEM. *N* = 3 independent experiments.

tyrosines (Fig. 1E and fig. S5). Together, our data indicate that LAT cluster formation is driven by dynamically rearranging, multivalent protein-protein interactions.

We compared the properties of LAT clusters in cells with those of reconstituted clusters in vitro and tested their functional importance. As in vitro, LAT microclusters in T cells sometimes fused with one another (fig. S3D). FRAP revealed that molecules exchange into and out of clusters in cells faster than in vitro (halftime of the recovery of 12 s versus 76 s), possibly due to different cluster size (see the supplementary text) or membrane fluidity. To assess valency dependence in cells, we expressed LAT tyrosine mutants with zero, one, two, three, or six Grb2 binding sites in a LAT-deficient Jurkat T cell line. A minimum of two Grb2 binding sites was required for robust cluster formation, and the degree of clustering increased with increasing number of phosphotyrosine sites (Fig. 2B). The degree of clustering correlated with activation of MAPK(ERK) (extracellular signal–regulated kinase) (Fig. 2C), suggesting that clustering of LAT and its partners is important for TCR signaling.

We used our in vitro assay to gain insight into the biochemical reactions that underlie the TCR signaling pathway. To LAT and its binding partners, we introduced the upstream signaling module consisting of (i) the cytoplasmic domain of the TCR subunit CD3ζ [which is sufficient to induce signaling in T cells (*21*)]; (ii) Lck, which phosphorylates the TCR; (iii) the cytoplasmic domain of the tyrosine phosphatase CD45, which opposes this reaction (*22*); and (iv) the protein kinase ZAP70, which is recruited to the phosphorylated TCR and phosphorylates LAT (*4*, *5*) (Fig. 3A). Initially, unphosphorylated LAT was evenly distributed on the membrane. After adenosine triphosphate (ATP) was added to initiate Lck phosphorylation of CD3ζ, ZAP70 was recruited to the membrane and LAT clustered (Fig. 3B and fig. S6A). ZAP70 was enriched in the clusters, as observed in T cells (*7*), whereas CD45 was excluded (Fig. 3B). The exclusion of CD45 was recapitulated in a simpler system in which clusters were formed by pLAT, Grb2, and Sos1 (Fig. 3C). The cytoplasmic domain of CD45 has a negative charge (isoelectric point 6.4). Assays with a series of differentially charged proteins revealed that, in general, positive charge favors inclusion into and negative charge favors exclusion from LAT clusters (fig. S7 and supplementary text). Consistent with limited access of CD45 to pLAT in the cluster center, CD45-mediated dephosphorylation of pLAT was reduced compared with that in unclustered conditions (Fig. 3D). In summary, our data demonstrate that LAT clusters are depleted in the phosphatase CD45 but enriched in the kinase ZAP70, which would be expected to promote LAT phosphorylation and increase the strength of TCR signaling.

We sought to integrate a downstream module that controls an important signaling output, actin polymerization (*23*, *24*). We attached His-tagged Lck, CD3ζ, and unphosphorylated LAT-Alexa647 to the supported lipid bilayer and added soluble ZAP70-505-Star, Gads, SLP-76, Nck, N-WASP (neuronal Wiskott-Aldrich syndrome protein), Arp2/3 (actin-related protein 2 and 3) complex, and rhodamine-labeled monomeric actin to the solution (Fig. 4A). Previous data have shown that Nck recruits N-WASP, which in turn activates the Arp2/3 complex to nucleate actin filaments (*16*, *25*). When ATP was added to initiate TCR phosphorylation, ZAP70 was recruited to the membrane, followed by LAT clustering and then actin polymerization from the LAT clusters (Fig. 4, B and C, and fig. S8). Later, when actin bundles formed, LAT clusters became rodlike and aligned with actin bundles (Fig. 4D and movies S4 and S5). This shape change is reversible, because clusters became round after depolymerization of F-actin by latrunculin A (fig. S9C). In summary, we show that actin polymerization is initiated from and can reorganize LAT clusters.

We next investigated whether clustering of Nck affects the efficiency of actin polymerization. In principle, actin polymerization could be stimulated by (i) recruitment of Nck from solution to the membrane, (ii) concentration and organization of Nck within clusters, or (iii) both effects. To isolate spatial distribution as a variable, we attached His_{10}-Nck to Ni-modified lipids in the planar bilayer and added soluble N-WASP, Arp2/3 complex, and actin. Increasing the density of Nck on the membrane resulted in a dose-dependent increase in assembly of actin (fig. S10). Using a density of Nck (150 molecules/μm^2) at which little actin polymerized, we tested whether clustering of Nck by pLAT, Gads, and pSLP-76 affected actin assembly. Clustering of Nck enhanced total actin assembly on the membrane by a factor of 6 (Fig. 4E). These results reveal that the clustering of actin regulators by LAT promotes actin polymerization beyond what can be achieved by recruitment to the membrane.

In summary, we reconstituted biochemical reactions of TCR signaling in an in vitro system, in which the components and their concentrations in the reaction can be controlled, rates can be measured, and molecular behaviors can be observed in ways that are difficult to achieve using intact cells. We observed multivalent assembly and consequent phase separation of LAT and its binding partners into liquid-like, micrometer-sized clusters. By manipulating clustering using LAT phosphorylation mutants, we show that clustering occurs through analogous mechanisms in vitro and in cells and that clustering promotes MAPK(ERK) signaling. Thus, as in three-dimensional phase separation (*17*, *26*), our results demonstrate that phase separation on membranes can create an environment that promotes biochemical reactions. LAT clusters excluded CD45 and retained ZAP70 to create an environment that perpetuated the phosphorylated state of LAT. Clustering of LAT promoted downstream biochemical reactions in the signaling pathway, specifically the ability of Nck to promote N-WASP–Arp2/3–mediated actin polymerization (fig. S11), as suggested by Nck density-dependent actin polymerization in cells (*27*). Multivalent interactions have been proposed to drive the assembly of many other cellular structures, including PML (promyelocytic leukemia) bodies, stress granules, and focal adhesions (*17*, *26*); thus, the mechanisms of spatial organization of biochemical reactions revealed here may apply to other cellular processes as well.

REFERENCES AND NOTES

1. H. Wu, *Cell* **153**, 287–292 (2013).
2. M. Bienz, *Trends Biochem. Sci.* **39**, 487–495 (2014).
3. A. K. Chakraborty, A. Weiss, *Nat. Immunol.* **15**, 798–807 (2014).
4. A. C. Chan, M. Iwashima, C. W. Turck, A. Weiss, *Cell* **71**, 649–662 (1992).
5. W. Zhang, J. Sloan-Lancaster, J. Kitchen, R. P. Trible, L. E. Samelson, *Cell* **92**, 83–92 (1998).
6. R. T. Abraham, A. Weiss, *Nat. Rev. Immunol.* **4**, 301–308 (2004).
7. S. C. Bunnell *et al.*, *J. Cell Biol.* **158**, 1263–1275 (2002).
8. A. D. Douglass, R. D. Vale, *Cell* **121**, 937–950 (2005).
9. R. Varma, G. Campi, T. Yokosuka, T. Saito, M. L. Dustin, *Immunity* **25**, 117–127 (2006).
10. K. L. Singleton *et al.*, *Sci. Signal.* **2**, ra15 (2009).
11. M. Y. Bilal, J. C. Houtman, *Front. Immunol.* **6**, 141 (2015).
12. M. L. Dustin, J. T. Groves, *Annu. Rev. Biophys.* **41**, 543–556 (2012).
13. J. C. Houtman *et al.*, *Nat. Struct. Mol. Biol.* **13**, 798–805 (2006).
14. M. Zhu, E. Janssen, W. Zhang, *J. Immunol.* **170**, 325–333 (2003).
15. Materials and methods are available as supplementary materials on *Science* Online.
16. L. Wunderlich, A. Faragó, J. Downward, L. Buday, *Eur. J. Immunol.* **29**, 1068–1075 (1999).
17. P. Li *et al.*, *Nature* **483**, 336–340 (2012).
18. S. Banjade, M. K. Rosen, *eLife* **3**, e04123 (2014).
19. A. Nag, M. I. Monine, J. R. Faeder, B. Goldstein, *Biophys. J.* **96**, 2604–2623 (2009).
20. M. Tinti *et al.*, *Cell Reports* **3**, 1293–1305 (2013).
21. B. A. Irving, A. Weiss, *Cell* **64**, 891–901 (1991).
22. E. Hui, R. D. Vale, *Nat. Struct. Mol. Biol.* **21**, 133–142 (2014).
23. S. Kumari *et al.*, *eLife* **4**, 04953 (2015).
24. S. C. Bunnell, V. Kapoor, R. P. Trible, W. Zhang, L. E. Samelson, *Immunity* **14**, 315–329 (2001).
25. R. Rohatgi, P. Nollau, H. Y. Ho, M. W. Kirschner, B. J. Mayer, *J. Biol. Chem.* **276**, 26448–26452 (2001).
26. A. A. Hyman, C. A. Weber, F. Jülicher, *Annu. Rev. Cell Dev. Biol.* **30**, 39–58 (2014).
27. J. A. Ditlev *et al.*, *J. Cell Biol.* **197**, 643–658 (2012).

ACKNOWLEDGMENTS

We thank S. Ross and L. Chang at Nikon Instruments for their loan of TIRF-capable microscopes, N. Stuurman for help with microscopy, A. Weiss for providing JCam2.5 cells, D. Liu for providing charged green fluorescent protein (GFP) constructs, C. Pak for providing charged GFP, J. Muller for providing intercellular adhesion molecule–1 protein, and L. Rice, X. Zeng, and members from the Vale Laboratory for comments on this manuscript. This work was supported by the HHMI's Collaborative Innovation Awards, NIH (R01-GM56322 to M.K.R.), and the Welch Foundation (I–1544 to M.K.R.). X.S. was supported by a Cancer Research Institute Irvington postdoctoral fellowship. J.A.D. was supported by National Research Service Award F32 (5-F32-DK101188). E.H. was supported as a fellow of the Leukemia and Lymphoma Society. J.O. was supported by funds from the Tobacco-Related Disease Research Program of the University of California (19FT-0090).

SUPPLEMENTARY MATERIALS

www.sciencemag.org/content/352/6285/595/suppl/DC1
Materials and Methods
Supplementary Text
Figs. S1 to S11
Tables S1 and S2
Movies S1 to S5
References (*28*–*32*)

3 December 2015; accepted 23 March 2016
Published online 7 April 2016
10.1126/science.aad9964

Phase separation of signaling molecules promotes T cell receptor signal transduction

Xiaolei Su, Jonathon A. Ditlev, Enfu Hui, Wenmin Xing, Sudeep Banjade, Julia Okrut, David S. King, Jack Taunton, Michael K. Rosen and Ronald D. Vale

Science **352** (6285), 595-599.
DOI: 10.1126/science.aad9964originally published online April 7, 2016

Phase separation organizes signaling

In T cell receptors, signaling molecules reorganize into tiny phase-separated droplets—like oil in water. Su *et al.* used an in vitro system with artificial membranes and 12 components of the T cell receptor signaling system to closely monitor the role of these molecular clusters (see the Perspective by Dustin and Muller). The clusters formed through phosphorylation-dependent association of the linker protein LAT (linker for activation of T cells) with other proteins. These clusters also managed to exclude an inactivating phosphatase and increased the specific activity of enzymes controlling actin polymerization.

Science, this issue p. 595; see also p. 516